Very low-energy nucleon-^{16}O coupled-channel scattering: Results with a phenomenological vibrational model

J. P. Svenne,[1,*] L. Canton,[2,†] K. Amos,[3,4,‡] P. R. Fraser,[5,§] S. Karataglidis,[4,3,‖] G. Pisent,[6,¶] and D. van der Knijff[3,#]

[1]*Department of Physics and Astronomy, University of Manitoba, and Winnipeg Institute for Theoretical Physics, Winnipeg, Manitoba, Canada R3T 2N2*

[2]*Istituto Nazionale di Fisica Nucleare, Sezione di Padova, Padova I-35131, Italy*

[3]*School of Physics, University of Melbourne, Victoria 3010, Australia*

[4]*Department of Physics, University of Johannesburg, P.O. Box 524 Auckland Park, 2006, South Africa*

[5]*Department of Physics, Astronomy and Medical Radiation Sciences, Curtin University, GPO Box U1987, Perth 6845, Australia*

[6]*Dipartimento di Fisica e Astronomia, Università di Padova, Padova, I-35131, Italy*

(Received 2 December 2015; revised manuscript received 29 December 2016; published 7 March 2017)

We employ a collective vibration coupled-channel model to describe the nucleon-^{16}O cluster systems, obtaining low-excitation spectra for ^{17}O and ^{17}F. Bound and resonance states of the compound systems have been deduced, showing good agreement with experimental spectra. Low-energy scattering cross sections of neutrons and protons from ^{16}O also have been calculated and the results compare well with available experimental data.

DOI: 10.1103/PhysRevC.95.034305

I. INTRODUCTION

We apply the multichannel algebraic scattering method (MCAS) to study the bound and resonance properties of the ^{17}O and ^{17}F nuclei below and above the nucleon-core threshold. With the same method, we investigate nucleon elastic scattering on ^{16}O at very low energies. We introduce as essential physics ingredients the coupling of the incident, or valence, nucleon with the low-lying collective vibrational states of the ^{16}O core. In the past, we considered many applications of the MCAS method describing couplings of valence nucleons with rotational states of the core. This is the first exploratory study where we consider collective vibrations in the MCAS method.

The approach we propose herein has some similarities and to a certain extent is complementary to the microscopic particle-vibration coupling (PVC) method developed recently to calculate scattering cross sections in light-medium nuclei. In the PVC method the collective core excitations are treated microscopically with the random-phase approximation (RPA) method, and one can find significant developments and applications along these lines in Refs. [1–5]. These microscopic type calculations are quite promising in the description of nucleon-nucleus collisions in the moderately low-energy range between 10 and 40 MeV, particularly in describing the particle-hole states as a doorway-state mechanism through which the flux evolves into more complex configurations such as overlapping states of the compound nucleus [1,5]. All these approaches, while successful at moderate energies, do not describe adequately the cross section in the very low-energy regimes (typically, lower than 5 MeV).

To consider nucleon scattering on ^{16}O in the very low-energy regime, we introduce a purely phenomenological description of excited states in terms of collective vibrations of the core nucleus. We use a geometrical model for particle-vibration couplings as has been discussed in textbooks [6]. We do not attempt to define the connection with the microscopic origin of the ingredients we use, but simply employ the basic Hamiltonian coupled-channel parameters in a fitting procedure. In addition, we consider couplings generated only by quadrupole and octupole phonons, which dominate the low-energy regime. These limitations, however, are not inherent to the MCAS approach. In the future it is feasible to apply the method to particle-vibration couplings generated microscopically, or to include additional multipolarities (for example, direct dipole or monopole excitation modes, etc.) that presently are not taken into account.

Previously, the MCAS method was developed and first applied [7] to the well-studied $n + {}^{12}$C system. That first MCAS investigation focused on obtaining excellent agreement with the experimental total elastic $n + {}^{12}$C cross section to $\sim$4 MeV, by varying free parameters of the potential used. With these same parameters, the spectrum of ^{13}C to $\sim$8 MeV also was well described for both bound states and resonances in the compound nucleus, ^{13}C. A number of MCAS studies on other nucleon-plus-nucleus systems have been carried out and published since then; see, e.g., Refs. [8–11]. In all of these studies, a rotational model was used to specify the matrix of coupled-channel interaction potentials for the nucleon with each target nucleus.

^{12}C is a partially-closed-shell nucleus in which the $0s_{\frac{1}{2}}$ state is expected to be fully occupied and the $0p_{\frac{3}{2}}$ and $0p_{\frac{1}{2}}$ states partially occupied. Conversely, the structures of ^{17}O and ^{17}F have been assumed to be that of a nucleon coupled to the ^{16}O core, with the latter defined as a closed $0p$ shell nucleus. That model yields the single-nucleon energies in the $0d1s$ shell model, which are obtained for the positive-parity

*svenne@physics.umanitoba.ca
†Corresponding author: luciano.canton@pd.infn.it
‡amos@unimelb.edu.au
§paul.fraser@curtin.edu.au
‖stevenka@uj.ac.za
¶w.pisent@gmail.com
#dvanderknijff@gmail.com

states of both ^{17}O and ^{17}F. Yet that model is too simplistic: the prevalence of low-lying negative-parity states in both mass-17 nuclei is a consequence of the ^{16}O core being far more complex: Brown and Green [12] had first realized that, at the minimum, a $4\hbar\omega$ shell model is needed to describe the spectrum of ^{16}O. Haxton and Johnston [13] had performed such a large-scale calculation, which was able to reproduce the positive-parity states of ^{16}O, especially the first-excited state, which is the 0_2^+ state at 6.06 MeV. Negative-parity states were calculated in Ref. [14] by using the same interaction and single-particle model space in a restricted $(1+3+5)\hbar\omega$ model space calculation. This idea is expanded in Appendix A, where a comparison is made of the spectrum obtained from the shell model and from MCAS.

In treating the coupling of a nucleon to the ^{16}O core, one must encompass the complicated multi-$\hbar\omega$ description of the core by a coupled-channel description, for which a vibrational model description of the states in ^{16}O is appropriate. Therefore, in Appendix B, we discuss in detail the particle-vibration coupling interactions to be used in the coupled-channel model.

As has been demonstrated in Ref. [8], solutions of the coupled-channel problem could have some spuriosity due to violation of the Pauli principle by single-nucleon orbit occupancies, in attaching the valence nucleon to states of the core that are already filled. However, it is possible to ensure that the Pauli principle is obeyed in coupled-channel problems by using orthogonalizing pseudopotentials (OPPs) [8,10]. Detailed clarification of this procedure is given in Refs. [8,15]. In the first calculations [7] of the nuclear system studied with MCAS, ($n+^{12}$C), Pauli blocking was required for the $0s_{\frac{1}{2}}$ and $0p_{\frac{3}{2}}$ neutron orbits. That study allowed all other orbits in the target states used to be accessible in the cluster solutions. More specifics are given in Ref. [7] and articles published subsequently [8,10,15].

To construct the couplings of a valence nucleon (or projectile) with a nucleus by using a geometric collective model, the coupling interactions are classified by coupling parameters, β_L. These parameters are required in a coupled-channel Hamiltonian for the coupling of the valence nucleon with the low-excitation states of the core nucleus. These β_L therefore, are not necessarily given from electromagnetic (EM) transition data of the core (because they involve also the interaction effects with the extra nucleon), but could be comparable to such. MCAS vibrational model results for the nucleon-^{16}O clusters are given in Secs. II and III where, in the former, coupling strengths β_L are allowed to be free parameters, and in the latter they are associated with deformations known from other data analyses. In Sec. IV we summarize the EM properties for ^{16}O to be expected with the described collective model.

Section V contains the conclusions.

II. MULTICHANNEL ALGEBRAIC SCATTERING THEORY RESULTS FOR $n+^{16}$O AND $p+^{16}$O SYSTEMS

We use as the primary nuclear interaction Hamiltonian (between the odd nucleon and the core) the following potential form:

$$V(r) = [V_0 + V_{ll}\{\mathbf{l}\cdot\mathbf{l}\} + V_{ss}\{\mathbf{I}\cdot\mathbf{s}\}]w(r) + 2\lambda_\pi^2 V_{ls}\frac{1}{r}\frac{\partial w(r)}{\partial r}\mathbf{l}\cdot\mathbf{s}. \quad (1)$$

A Woods–Saxon shape, $w(r) = [1+\exp(\frac{r-R_0}{a})]^{-1}$,has been used. The vector operators $\mathbf{l}$,$\mathbf{s}$,$\mathbf{I}$ denote orbital, nucleon spin, and target spin, respectively.

The interaction contains operator components with zero, first, and second order irreducible terms due to the expansion of the vibration (or deformation) operator. For each term in the interaction, the coupled-channel expressions in the channel-coupling scheme can be given as

$$V_{cc'}(r) = \{V^{(0)}(r)\}_{cc'} + \left\{V^{(1)}(r)\sum_\lambda \mathcal{Q}_\lambda^{(1)}\cdot Y_\lambda(\theta\phi)\right\}_{cc'} + \left\{V^{(2)}(r)\sum_\lambda\left[\sum_{l_1 l_2}\mathcal{Q}_\lambda^{(2)}(l_1,l_2)\right]\cdot Y_\lambda(\theta\phi)\right\}_{cc'}. \quad (2)$$

The approach is explained in full detail in Appendix B. The importance of including second-order terms in the deformation expansion of the interaction has been discussed in Ref. [16].

In coordinate space, if those potentials are designated by local forms $V_{cc'}(r)\delta(r-r')$, the application of OPP method requires considering the solutions of the Schrödinger equation with the generalized nonlocal potential

$$\mathcal{V}_{cc'}(r,r') = V_{cc'}(r)\delta(r-r') + \lambda_c A_c(r)A_c(r')\delta_{cc'}, \quad (3)$$

where $A(r)$ is the radial part of the single-particle bound-state wave function in channel c spanning the phase space excluded by the Pauli principle. The OPP method takes into account the Pauli forbidden states in the limit $\lambda_c \to \infty$, and for practical use $\lambda_c = 10^6$ MeV suffices. But we take into account also more general configurations with smaller values for λ_c as extensively discussed in Refs. [10,15].

The full set of parameters that defines the interaction potential is given in Table I.

MCAS calculations were carried out for $n+^{16}$O, using five target states in ^{16}O; namely, the 0^+ ground state ($E=0$ MeV), the second 0^+ state ($E=6.049$ MeV), the first 3^- state ($E=6.1299$ MeV), the first 2^+ state ($E=6.9171$ MeV), and the first 1^- state ($E=7.1169$ MeV). These states, along with the corresponding Pauli blocking or hindrance strengths are listed in the lower section of Table I. The use of blocking strengths with dimensions of energy is typical of approaches that use the OPP method; a method that is not restricted only to nuclear physics applications. It was applied also in studies of the electronic structure of atoms to eliminate unwanted states in bound [18] and scattering [19] problems. In the table, the blocking strengths are given in MeV.

The 2_1^+ and 3_1^- states are considered to be single-phonon states. In the present model, we include also the couplings of the excited 0_2^+ and 1_1^- states to the 0_1^+ ground state, but only as a second-order effect in the coupling parameters (see Appendix B). We did not include couplings with direct excitation modes described by monopole or dipole operators.

TABLE I. Parameter values for $n + {}^{16}$O and $p + {}^{16}$O MCAS cluster structure. The potential parameters, V_0, $V_{\ell\ell}$, $V_{\ell s}$, V_{ss}, have different values: if they act on negative or positive orbital parity states, $P = -$ or $P = +$, respectively. The lower part of the table describes the λ_c parameters of the OPP term.

V_x (MeV)	$P=-$	$P=+$	Geometry	Value	Coulomb [17]
V_0	−47.15	−50.6	R_0	3.15 fm	$R_c = 2.608$ fm
$V_{\ell\ell}$	2.55	0.0	a	0.65 fm	$a_c = 0.513$ fm
$V_{\ell s}$	6.9	7.2	β_2	0.21	$w = -0.051$
V_{ss}	2.5	−2.0	β_3	0.42	
I_n^π	E_n (MeV)	$0s_{\frac{1}{2}}$	$0p_{\frac{3}{2}}$	$0p_{\frac{1}{2}}$	$0d_{\frac{5}{2}}$
0_1^+	0.0	10^6	10^6	10^6	0.0
0_2^+	6.049	10^6	10^6	0.0	0.0
3_1^-	6.13	10^6	10^6	5.0	0.0
2_1^+	6.92	10^6	10^6	0.0	0.0
1_1^-	7.12	10^6	10^6	5.0	1.0

In this sense the model approach used here is more schematic than the microscopic approach used in Ref. [20]. However, that microscopic approach was designed to describe excitations of giant-type resonances which are located at higher energies.

All the other potential and geometric parameters used for the present nucleon + ^{16}O calculations are given in the upper part of Table I. We note that the value of β_2 in the table is small compared with values required in assessment of a $B(E2)$ value in ^{16}O [21] and later, in the next section, we consider the effects of setting the deformation parameter in MCAS evaluations to match the electromagnetically determined value.

The MCAS results found with this parameter set of Table I are compared with the known spectra of ^{17}O (left columns) and of ^{17}F (right columns) in Fig. 1. There are more evaluated

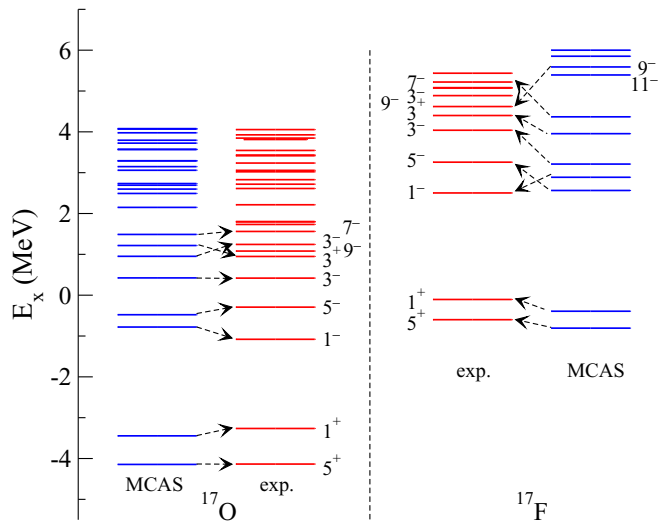

FIG. 1. Spectra of ^{17}O (left panel) calculated with MCAS and experimental and of ^{17}F (right panel) using the parameter set of Table I. The numbers by the levels are twice the spin of the level, and the superscript indicates the parity. The zero on the scale is at the respective $n + {}^{16}$O and $p + {}^{16}$O thresholds.

levels found at higher energies than shown. Good agreement between theory and data at low energies is now obtained for both nuclear systems.

A. Bound and resonant states in ^{17}O and ^{17}F

In Table II, we give the spin-parity values, the data, and MCAS results for ^{17}O and the data and MCAS results for ^{17}F for the lowest 30 levels of each. The oxygen list is sorted in increasing energy of the experimental values. In Table II, the column for the measured ^{17}F levels are always associated with a J^π value, even though some measured values have unknown J^π. In those cases where the association of J^π is purely speculative, the energy levels are endowed with an asterisk. Note that the experimental widths are full widths at half maximum, and are total widths, while the MCAS widths $\Gamma_{\rm mcas}$ represent only nucleon-emission widths. There are clear mismatches in the lists, but it is noteworthy that of the thirty levels listed for ^{17}O and ^{17}F, twenty in ^{17}O and twenty-four in ^{17}F, have matching experimental and MCAS-evaluated partners within one MeV in excitation of each other. Furthermore, the majority of the larger mismatched pairs lie above 7 MeV in excitation and we expect that coupling of additional target states to those used would have more influence with increasing excitation in the clusters.

A measure of the overall agreement is the root-mean-square value,

$$\mu_N = \sqrt{\frac{\sum_{n=1}^{N}[E_{\rm expt}(n) - E(n)]^2}{N}}, \tag{4}$$

where N is the number of bound states and resonance centroid energies considered and $E_{\rm expt}(n)$ and $E(n)$, respectively, are the experimental and calculated values of the bound and resonance centroid energies in the set. The root-mean-square value, Eq. (4), for the calculated levels in ^{17}O, considering the lowest 30 energy levels is $\mu_{30} = 1.2371$ MeV, and with just the lowest 20 levels, $\mu_{20} = 1.1240$ MeV.

To study the mirror system to $n + {}^{16}$O; namely, $p + {}^{16}$O leading to the compound system ^{17}F, we use the same parameter set as in Table I with the addition of the Coulomb interaction. (A Coulomb potential has been generated from the charge distribution assumed for ^{16}O.) The charge distribution of the protons in ^{16}O is described by a three-parameter Fermi charge distribution geometry given by

$$\rho_{ch}(r) = \rho_0 \frac{1 + w\left(\frac{r}{R_c}\right)^2}{1 + \exp\left(\frac{r - R_c}{a_c}\right)}, \tag{5}$$

where the parameters R_c, a_c, and w were obtained from experiment to have the values [17] given in the top of the last column of Table I. For ^{17}F, the comparison with experiment shown in Fig. 1, is even better than for ^{17}O, giving $\mu_{30} = 1.0419$ and $\mu_{20} = 0.9201$ for the 30 and 20 lowest states, respectively. However, since a number of the higher-energy levels observed in ^{17}F have not been given experimentally known spin-parities, we have made an arbitrary association between some measured and calculated levels.

With respect to the small Coulomb residual displacement energy of 208 keV between the experimentally known value for

TABLE II. The 30 lowest levels in ^{17}O and ^{17}F, experiment and theory. Energy levels are in MeV, widths in keV.

J^π	^{17}O: E_{expt}	Γ_{expt}	^{17}O: E_{mcas}	Γ_{mcas}	^{17}F: E_{expt}	Γ_{expt}	^{17}F: E_{mcas}	Γ_{mcas}
$\frac{5}{2}^+$	−4.1436		−4.1432		−0.6005		−0.8079	
$\frac{1}{2}^+$	−3.27287		−3.4426		−0.10517		−0.3927	
$\frac{1}{2}^-$	−1.08824		−0.7781		2.5035	19	2.8874	5.58×10^{-5}
$\frac{5}{2}^-$	−0.30084		−0.4792		3.2565	1.5	2.5644	9.80×10^{-6}
$\frac{3}{2}^-$	0.4102	40	0.4226	1.2768	4.0395	225	3.2104	0.00552
$\frac{3}{2}^+$	0.9412	96	0.9534	129	4.3995	1530	3.9557	0.906
$\frac{9}{2}^-$	1.0722	<0.1	2.1528	1.08×10^{-7}	4.6195		5.3930	1.26×10^{-9}
$\frac{3}{2}^-$	1.2356	28	2.7332	0.2923	4.8875	68	5.8526	6.78×10^{-5}
$\frac{7}{2}^-$	1.55366	3.4	1.2185	0.1615	5.0715	40	4.3679	1.954×10^{-3}
$(\frac{5}{2}^-)$	1.5892	<1	3.1504	0.1982	5.0815*	<0.6	6.3027	6.8×10^{-4}
$\frac{3}{2}^+$	1.7255	6.6	4.0680	40.226	5.2195	180	7.3661	0.0484
$\frac{1}{2}^-$	1.7954	32	3.5670	26.51	5.4365	30	6.6181	0.0302
$\frac{1}{2}^+$	2.2124	124	3.0612	0.3541	5.9595	200	6.0004	0.212
$(\frac{5}{2}^+)$	2.7184	<1	2.6958	8.3616×10^{-2}	5.9790*	<1.6	5.6928	1.25×10^{-4}
$(\frac{7}{2}^-)$	2.8284	<1	2.4923	0.8880	6.9455*	30	5.6906	0.0039
$\frac{5}{2}^-$	3.0221	1.38	3.7962	1.0455	6.4265	3.8	6.5382	1.216×10^{-3}
$\frac{3}{2}^+$	3.0584	280	4.9729	53.98	6.7555	10	7.6222	0.0790
$\frac{5}{2}^+$	3.2356	0.64	3.2894	4.8518	7.3495*	10	6.3457	0.00808
$\frac{5}{2}^-$	3.2386	0.96	4.9148	0.1685	7.7825*	11	8.0635	0.00666
$\frac{3}{2}^-$	3.4154	500	4.0794	0.4399	6.1735*	4.5	7.7045	1.46×10^{-3}
$(\frac{7}{2}^+)$	3.4324	<0.1	3.2902	2.58×10^{-3}	6.8705	5	6.6024	1.304×10^{-5}
$\frac{7}{2}^-$	3.5446	14.4	4.5986	1.2018	7.4095	50	7.7624	0.01786
$\frac{11}{2}^-$	3.6134		1.4902	7.5970×10^{-6}	6.8475*	<5	4.7564	5.44×10^{-7}
$\frac{1}{2}^+$	3.8124	90	3.7228	228	7.1495	179	7.0725	267
$\frac{1}{2}^-$	3.8469	270	4.8343	21.55	7.4745		7.4661	0.0454
$\frac{3}{2}^+$	3.9264	85	5.3846	0.8878	6.8785	795	8.8502	24.7
$\frac{3}{2}^-$	4.0564	60	5.4326	13.8864	7.5995*	700	7.7045	8.4175
$\frac{1}{2}^+$	4.1988	11.4	6.8393	99.201	7.8155	45	10.1828	366
$\frac{5}{2}^+$	4.2587	6.17	3.9770	25.782	7.4695*	100	7.2445	26.53
$\frac{9}{2}^+$	4.3224	2.13	2.5973	0.0711	6.8535	7	5.9439	0.3759

the ground state of ^{17}F and that calculated by MCAS, changing to smaller values of R_c and a_c does make the gap smaller. But unless quite unrealistic values are used, it is not enough to explain observation. Possibly a residual gap reflects effects of charge symmetry breaking in the underlying two-nucleon interactions [22,23]. This gap is comparable with those found in other mirror systems studied in Ref. [23].

B. Nucleon-scattering cross sections from ^{16}O

The total $n + {}^{16}$O scattering cross section has been calculated by using MCAS as a function of neutron energy to 8.0 MeV by using the parameter set in Table I. In Fig. 2 the results are compared with data on a logarithmic energy scale. This emphasizes the very low-energy values and reveals that the calculated cross sections agree with observation very well at energies $\leqslant$1 MeV. The first large resonance, labeled $\frac{3}{2}^-$ is in the correct position in the MCAS result, but its width is much smaller than the experimental one. This resonance decays both by γ and neutron emission but the radiative width is only 1.8 ± 0.35 eV [28]. The neutron width has been assessed [29] to be ∼40 keV by analysis of the elastic neutron-scattering cross sections from ^{16}O. The higher-energy regime is best shown on a linear scale, as done in Fig. 3. It shows considerable structure in the MCAS results, and resonances are predicted to exist where experiment reveals some, but the precise matching of resonances in the 3–4 MeV region is not as good as one would like, while the background cross section is matched

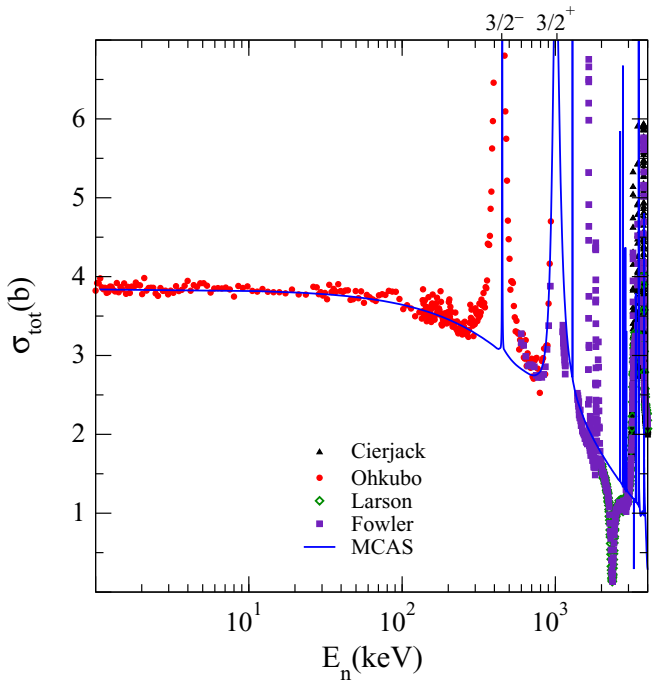

FIG. 2. Total neutron scattering from ^{16}O calculated with MCAS (solid line) using the parameter set in Table I compared with four data sets. The circles are data from Ohkubo [24], the triangles are data from Cierjacks *et al.* [25], the squares are from Fowler *et al.* [26], and the diamonds are from Larson *et al.* [27]. The energy scale is *logarithmic*, in units of keV.

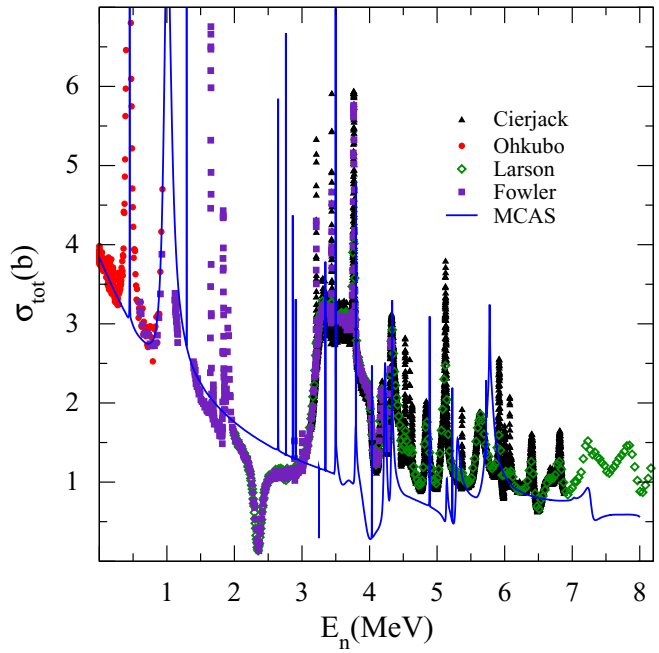

FIG. 3. Same as in Fig. 2 but with a linear scale.

fairly well. As the higher-energy region occurs at ∼8 MeV excitation in the compound nucleus, to improve on these cross-section results, more target states in ^{16}O are probably needed in MCAS calculations.

Next we consider the scattering cross section for $p + {}^{16}$O. In Fig. 4, differential cross sections at three different scattering angles are shown as a function of energy from 0 to 2.0 MeV with data from Braun and Fried [30]. The next two figures 5 and 6 show some $p + {}^{16}$O scattering results from Ramos [31], at two angles, together with MCAS results at the angles used in the Ramos work. For comparison, some calculated with MCAS at other angles are shown. There is reasonable agreement between the MCAS results and the data, and the calculated results show a measurable variation with energy and angle as well as possible resonance attributes. Reasonable agreement between MCAS results and data is seen.

III. EFFECT OF VARIATIONS OF β_L PARAMETERS

In Table I we presented the set of parameters that were used for the MCAS calculations of neutron and proton scattering from ^{16}O to obtain the results of Figs. 1–6, and Table II. Not all the parameters in Table I were treated equally. Those fitted are, essentially, the interaction strengths (V_0, $V_{\ell\ell}$, $V_{\ell s}$, V_{ss}) and the β_2 and β_3 coupling parameters. In contrast, the radius and diffuseness, R_0 and a, have been held fixed. According to the analysis discussed in Ref. [32], R_0 denotes the Hamiltonian nucleon-nucleus interaction radius, which is different from the charge radius R_c of ^{16}O taken from Ref. [17]. In the calculation shown in Table II and Figs. 1–6, the β_2 and β_3 parameters were adjusted to the values given in Table I to get optimal results in the coupled-channel calculations. However, as an alternative to this approach, β_2 and β_3 could also be linked to the experimental $B(E2)$ and $B(E3)$ values, which lead to

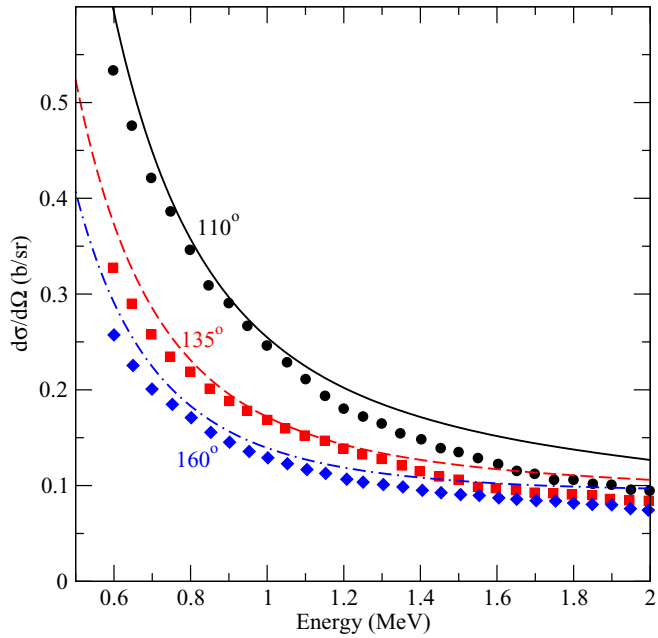

FIG. 4. Differential scattering cross sections of protons from ^{16}O calculated with MCAS, compared with data sets from Braun and Fried [30] at three scattering angles. The solid, dashed, and dot-dashed lines are the MCAS results at the angles shown. The circles, squares, and diamonds are data points at the corresponding angles shown.

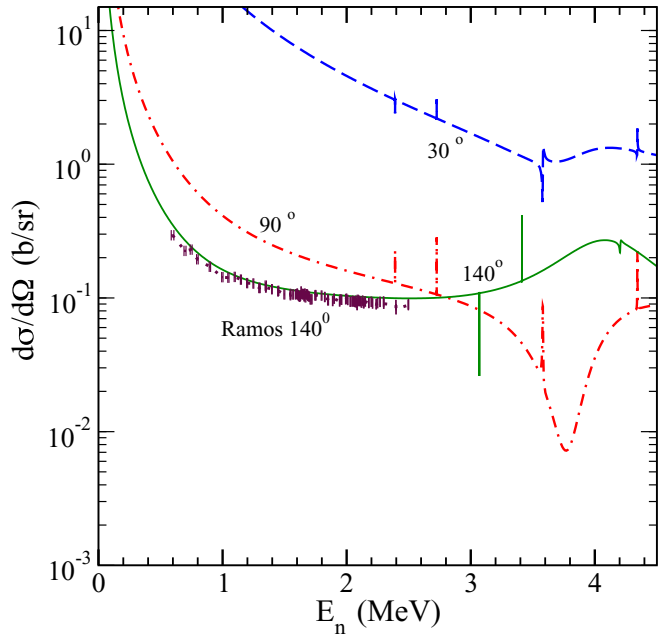

FIG. 5. Differential scattering cross sections of protons from ^{16}O calculated with MCAS, compared with a data set from Ramos *et al.* [31] at a scattering angle of 140°.

$\beta_2 = 0.362 \pm 0.018$ [21,33,34] and similarly to a value of 0.6 for the octupole coupling β_3 [35]. Therefore, with the aim to consider this alternative option, we made a new calculation fixing $\beta_2 = 0.36$ and $\beta_3 = 0.6$ and refitting the remaining adjustable parameters. The varied list of parameters values is reported in Table III.

A distinctive feature of the model couplings discussed in Appendix B is that the ^{16}O 0^+ and 1^- excited states

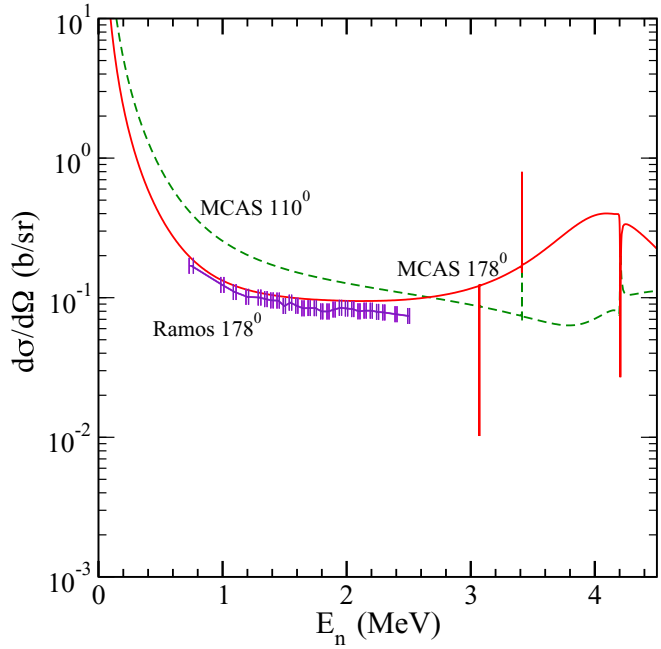

FIG. 6. As in Fig. 5, compared with a data set from Ramos *et al.* [31] at a scattering angle of 178°.

TABLE III. New parameter values for $n + {}^{16}$O MCAS cluster structure.

V_x (MeV)	$P = -$	$P = +$	Geometry	Value	
V_0	−45.0	−45.0	R_0	3.15 fm	
V_{ll}	0.55	−0.216	a	0.65 fm	
V_{ls}	8.71	8.71	β_2	0.36	
V_{ss}	2.0	1.9	β_3	0.6	
I_n^π	E_n (MeV)	$0s_{\frac{1}{2}}$	$0p_{\frac{3}{2}}$	$0p_{\frac{1}{2}}$	$0d_{\frac{5}{2}}$
0_1^+	0.0	10^6	10^6	10^6	0.0
0_2^+	6.049	10^6	10^6	0.0	0.0
3_1^-	6.13	10^6	10^6	5.0	1.0
2_1^+	6.92	10^6	10^6	0.5	0.0
1_1^-	7.12	10^6	10^6	5.0	1.0

are coupled through second-order couplings of quadrupole-octupole vibrations. This choice is very specific for the schematic model considered herein. Other possible excitation-de-excitation modes (e.g., monopole or dipole couplings) are not contemplated in the model given in Appendix B. To estimate the effect of those two states and their couplings, we compare the full (five-state) calculation with a calculation where the couplings to the 0^+ and 1^- excitations have been removed. This alternative calculation is denoted as a three-state calculation (0^+gs, 3^-, 2^+) in Figs. 7 and 8.

In Fig. 7 we illustrate the bound and resonant spectra of ^{17}O when the β couplings have been set at the adopted values. The

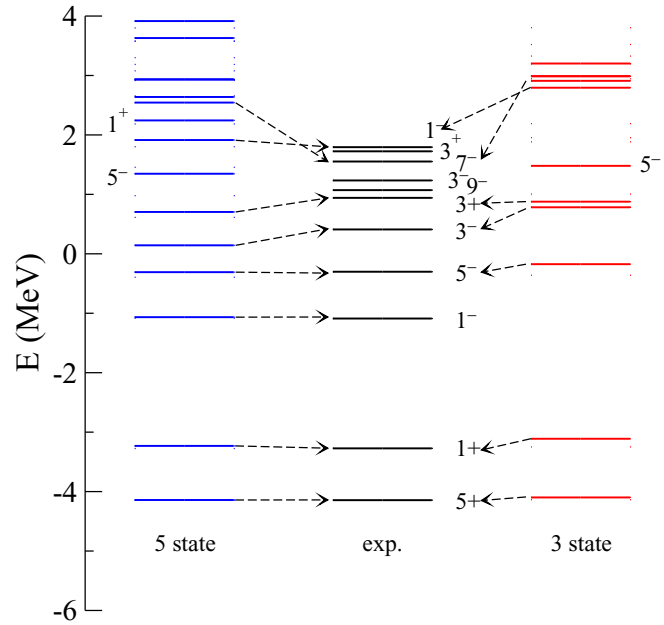

FIG. 7. Spectra of ^{17}O, left and right are calculated with MCAS including and excluding the two states 0^+ and 1^-. The middle column represents the experimental spectrum. The calculations have been performed with $\beta_2 = 0.36$ and $\beta_3 = 0.6$, according to Table III. The numbers by the levels are twice the spin of the level, and the superscript indicates the parity. The zero on the scale is at the $n + {}^{16}$O threshold.

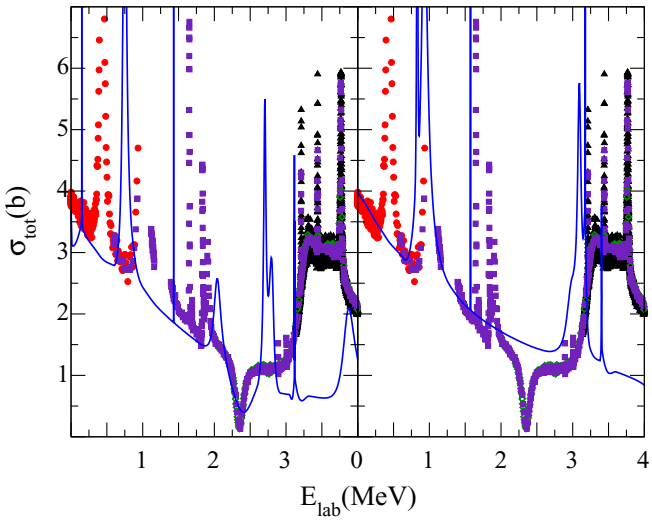

FIG. 8. Total neutron scattering from ^{16}O calculated with MCAS (solid line), utilizing the parameter set in Table III (using $\beta_2 = 0.36$ and $\beta_3 = 0.6$). Left panel refers to a five-state calculation while right panel refers to a three-state calculation (0^+gs, 3^-, 2^+). The experimental data are the same as for Fig. 2.

results on the left column refer to the five-state calculation, while the results in the right column refer to the corresponding three-state calculation. The middle column contains the known experimental data. Note that the two calculated results are quite similar except that, with the three-state calculation, we completely miss the second excited state $(\frac{1}{2})^-$. In Fig. 8, we show the neutron-oxygen total scattering cross section obtained from the same variation of the β_2 as used for Fig. 7 for the two model (three-state and five-state) calculations. There are small but significant differences between the results shown in Fig. 2 and in Fig. 8; the former showing a near-perfect agreement between data and MCAS (with $\beta_2 = 0.21$ and $\beta_3 = 0.42$). It is not clearly understood if one should use for these β_L values those deduced from (electromagnetic) experiments with ^{16}O, as in Fig. 8, or if the nucleon interaction leads to some modification of these deformation values in the coupled-channel dynamics. After all, the interaction radius itself is affected by the presence of the incoming nucleon, as discussed in Ref. [32], and leads us to use a value which is different from the charge radius of the ^{16}O target. The same could happen for the β parameters.

IV. SUMMARY OF ELECTROMAGNETIC TRANSITIONS

Finally, we present here a summary of the EM transitions in ^{16}O that can be obtained with the collective model we employ. In particular, the $E0$, $E2$, and $E3$ transition properties between some of these states have been assessed; data on those of prime interest are as listed in Table IV.

The $E2 : 0_1^+ \rightarrow 2_1^+$ values given in Ref. [21] span a wide range and all have been extracted from experimental data. However, the value 40.6 e^2 fm^4 has been adopted. With that value, and assuming for ^{16}O a uniform spherical charge density in its ground state (radius $R = 1.2A^{1/3}$ fm), the base vibration

TABLE IV. Electromagnetic transition properties in ^{16}O.

Type	Transition	Model result	Expt. value	Reference
$\rho^2(E0)$	$0_2^+ \rightarrow 0_1^+$	0.026	0.153	[36]
$B(E2)$	$0_1^+ \rightarrow 2_1^+$	40.6 (e^2 fm^4)	23–51 (e^2 fm^4)	[21]
$B(E3)$	$0_1^+ \rightarrow 3_1^-$	900 (e^2 fm^6)	400–1550 (e^2 fm^6)	[35]

model gives the deformation parameter as [21]

$$\beta_2 = \frac{4\pi}{3ZR_0^2}\sqrt{B(E2 : 0_1^+ \rightarrow 2_1^+)} = 0.36 \text{ for } ^{16}\text{O}\,. \quad (6)$$

With the same model geometry, for ^{16}O, and using the link [37] between $\rho(E0 : 0_2^+ \rightarrow 0_1^+)$ and the $B(E2 : 2_1^+ \rightarrow 0_1^+)$,

$$\rho(E0 : 0_2^+ \rightarrow 0_1^+) = \sqrt{10}\frac{4\pi}{3}\frac{1}{Ze^2R_0^4}B(E2 : 2_1^+ \rightarrow 0_1^+), \quad (7)$$

and so the square is

$$\rho^2(E0 : 0_2^+ \rightarrow 0_1^+) = \frac{320\pi^2}{9Z^2e^4R_0^8}[B(E2 : 2_1^+ \rightarrow 0_1^+)]^2 = 0.026, \quad (8)$$

a factor of ∼6 smaller than observed. Of course the structure model considered is simplistic, with phenomena such as shape coexistence and noncollective attributes known to influence monopole strengths. For the same reason, our simple vibration model gives zero for the direct isoscalar $E1$ matrix element.

Likewise the $E3 : 0_1^+ \rightarrow 3_1^-$ values given in Ref. [35] span a wide range and all have been extracted from experimental data. We use an average value of 900 e^2 fm^6 with which the basic vibration model for ^{16}O gives the deformation parameter $\beta_3 = 0.6$.

With reference to ^{16}O, it is well known that a $E1$ transition from a 1^- to the 0^+ ground state (gs) has been observed with an extremely small transition probability (see Refs. [38–40] and references therein). However, this is not accounted for in this study, or in most other investigations to date (see Ref. [41] for an investigation into the underlying causes).

V. CONCLUSIONS

The MCAS method for nucleon-nucleus scattering studies was developed and first used for neutron scattering from the well-known nucleus ^{12}C [7]. The structure of that target nucleus was described by a rotational model with a deformed Fermi function, with the deformation specified by a β_L value. The parameters of the system were chosen to obtain a very good description of the neutron-^{12}C elastic-scattering cross section. This study also yielded a good description of the energy levels in ^{13}C, both bound states and resonances. Since that first result, a number of other nucleon + nucleus systems have been evaluated and studied by the MCAS method, all using the rotational model.

In this work the MCAS method has been applied for the first time with a vibrational model for the target nucleus to study nucleon scattering on the ^{16}O nucleus. The spectra of ^{17}O and of ^{17}F have been evaluated by using the MCAS approach, treating these nuclei as $n + {}^{16}$O and $p + {}^{16}$O compounds, respectively.

As the main result, we have shown that, with this approach, it is possible to describe the very low-energy cross section for neutron and proton elastic scattering on ^{16}O with a coupled-channel model that takes into account the excitation dynamics of the low-lying collective states of ^{16}O. The calculation performed and the results obtained show that the approach has potential interest for any application where the determination of low-energy cross section is of great importance. For instance, the low-energy regime is of import for capture cross sections [42], as well as for nuclear reactor physics applications [43].

It must be observed that the vibrational coupled-channel model in its present form is still at a preliminary stage, and that a variety of improvements can be performed in future studies. For example, the use of fit parameters typical of a macroscopic theory can be reduced if not fully removed if we use insights coming from microscopic theories. This is especially so if one uses ground-state densities coming from folding model calculations, and in a similar manner one derives the transition densities for the coupling interactions. However, at present there is no microscopic (or microscopically inspired) theory that works so well in this low-energy scattering regime. Another improvement could consider couplings to the excited 0^+ and 1^- states derived directly from first-order transitions of monopole, dipole structure, while in the present model we take into account for these states only second-order transitions of quadrupole plus octupole type. With these caveats, we have described the neutron or proton $+{}^{16}$O coupled-channel dynamics by using the five lowest excited states in ^{16}O with the interaction potentials specified by a collective vibration model for the target states. With those interactions, the Pauli principle was satisfied by using the orthogonalizing pseudopotential scheme [9], and then good agreement between theory and data at low energies was found. While there remain discrepancies, such as a small residual displacement energy, of thirty levels listed in Table II for ^{17}O and ^{17}F, twenty in ^{17}O and twenty-four in ^{17}F have matching MCAS evaluated partners within one MeV in excitation of each other.

The total elastic-scattering cross section for neutrons on ^{16}O is a near perfect match to data up to 1 MeV of excitation, except for the widths of the first two peaks around 1 MeV. At higher energy there are additional resonances in the MCAS results, which, however, only approximately match available data. For the scattering of low-energy protons from ^{16}O, differential cross sections only exist at fixed scattering angles. Our calculated results agree very well with measured ones.

ACKNOWLEDGMENTS

S.K. acknowledges support from the National Research Foundation of South Africa. J.P.S. acknowledges grant support from NSERC, Canada, during the early part of this work.

APPENDIX A: SHELL-MODEL CONSIDERATIONS FOR ^{16,17}O AND ^{17}F

If ^{16}O is considered to be a doubly magic nucleus, in its ground state the $0s_{\frac{1}{2}}$ and both orbits in the $0p$ shell will be fully occupied and that state would be predominantly spherical in shape. The two nuclei, ^{17}O and ^{17}F, often have been considered as a single nucleon outside an ^{16}O core, and as mirror nuclei with the first three positive-parity states reflecting the single-particle energies of the $0d_{\frac{5}{2}}$, $1s_{\frac{1}{2}}$, and $0d_{\frac{3}{2}}$ levels in the $(0d1s)$ shell model. But the model for each nucleus is not so simple: in a $(0+2)\hbar\omega$ shell-model prescription there is significant admixing of $2\hbar\omega$ components, $\sim$25%, in the ground states. This largely stems from $2p$-$2h$ components giving rise to additional nucleons in the $(0d1s)$ shell. With this in mind, it is instructive to compare the extreme shell-model picture, with one particle in the $(0d1s)$ shell, or the more general $(0+2)\hbar\omega$ model, to the collective model description contained in MCAS theory [7], which describes low-energy nucleon-nucleus scattering, and the spectrum of the compound system (both bound states and resonances). However, it is well known that the description of the spectrum of ^{16}O requires a $4\hbar\omega$ shell model at the minimum [12–14]. We discuss aspects of both the $2\hbar\omega$ and $4\hbar\omega$ shell-model results for ^{16}O to frame the discussion of the $2\hbar\omega$ results we have been able to obtain, so far, for the mass-17 systems.

Haxton and Johnson [13] made a $(0+2+4)\hbar\omega$ shell-model calculation of the spectrum of ^{16}O. They used a two-nucleon interaction that consisted of

1. the Cohen and Kurath (8-16)2BME [44] for the $0p$ shell;
2. the Brown and Wildenthal interaction [45] for the $(0d,1s)$ shell;
3. the Millener–Kurath interaction [46] for the $(0p,0d,1s)$ cross shell elements;
4. the bare Kuo g matrix for the $2\hbar\omega$ interaction [47,48].

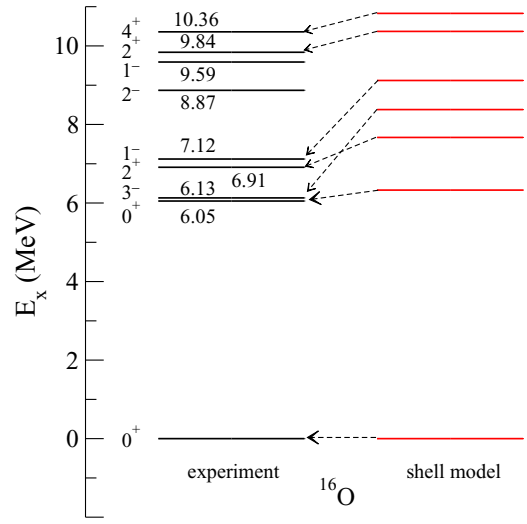

FIG. 9. The low-lying spectrum of ^{16}O. The experimental energies [29] are compared with the shell-model results found by using the Haxton and Johnson interaction.

TABLE V. Shell occupancies (proton + neutron) in the ground state of ^{16}O.

Orbital	$0s_{\frac{1}{2}}$	$0p_{\frac{3}{2}}$	$0p_{\frac{1}{2}}$	$0d_{\frac{5}{2}}$	$0d_{\frac{3}{2}}$	$1s_{\frac{1}{2}}$	$0f_{\frac{7}{2}}$	$0f_{\frac{5}{2}}$	$1p_{\frac{3}{2}}$	$1p_{\frac{1}{2}}$
$(0+2)\hbar\omega$	3.999	7.741	3.788	0.283	0.135	0.021	0.0	0.0	0.028	0.005
$(0+2+4)\hbar\omega$	3.996	7.319	3.262	0.831	0.441	0.138	10^{-3}	7×10^{-4}	0.003	0.002

Every other matrix element necessary to specify the interaction in the complete model space was set to zero. Furthermore, those matrix elements which gave rise to the violation of the Hartree–Fock condition were also removed. In that sense, the interaction was not complete for the model space assumed. Nevertheless, the spectrum they obtained was reasonable and confirmed the Brown and Green result. An extension of that shell-model calculation to include negative-parity states [14] also found reasonable agreement for the states in the spectrum. While the single-particle basis assumed was complete for the $(0+2+4)\hbar\omega$ space for the calculation of the positive-parity states, there was one restriction in the calculation of the negative-parity states, which was done in the same single-particle basis. That restriction did not allow for the single-particle excitations to the $0i1g2d3s$ shell.

Haxton and Johnson sought to determine whether the Brown and Green model [12], which placed importance on inclusion of $4\hbar\omega$ components in the wave functions for ^{16}O, could be reproduced with a microscopic shell-model calculation. With this scheme, the states of ^{16}O have been determined by using the Haxton version of the GLASGOW shell-model program [14] and the results of that [14] are shown in Fig. 9. Therein, while the positive-parity states were evaluated in a complete $(0+2+4)\hbar\omega$ space by using the Haxton and Johnson interaction, the negative-parity states were evaluated in a (restricted) $(1+3+5)\hbar\omega$ space, using the same interaction. Both calculations used the single-particle basis from the $0s$ shell up to and including the $(0h1f2p)$ shell. The restriction placed in the $(1+3+5)\hbar\omega$ space is that single-particle excitations from the $0p$ shell up to the $(0i1g2d3s)$ shell were excluded. This restriction does not guarantee complete removal of center of mass spuriosity but, as the center-of-mass energy for all states obtained in the model is 19.19 MeV, there is very little spuriosity in the specified low-lying states.

All positive-parity states displayed in Fig. 9 are well reproduced by the calculation, but the 3^- and 1^- are not, lying about 2 MeV above the experimental values. The predicted energies of the 2^- and 1_2^- states are at 12.67 and 15.97 MeV, respectively, and so are not shown in the figure.

A complete $(0+2)\hbar\omega$ calculation, using the MK3W interaction, was made for the positive-parity states of ^{16}O as well. That calculation placed all excited states above 20 MeV, indicating the importance of including $4\hbar\omega$ components to give a sensible mixing of $2\hbar\omega$ and $4\hbar\omega$ components when a $2\hbar\omega$ interaction is involved; bringing the energies of states into better agreement with experiment. The summed shell occupancies (proton and neutron are identical) of the ground state in ^{16}O from the two shell-model calculations are listed in Table V.

Higher orbits in the $(0+2+4)\hbar\omega$ space have occupancies less than 10^{-5} nucleons. From these numbers it is clear that the significant populations in the $(0d1s)$ shell and the lack of population in the higher shells indicates that the ground state is essentially of $(0+2)\hbar\omega$ character, although the distribution in the lower shells is affected by the $4\hbar\omega$ contributions.

As the ground state of ^{16}O is so dominantly of $(0+2)\hbar\omega$ character, we have calculated the spectra of ^{17}O and ^{17}F in that model space, for the positive-parity states, and in a restricted $(1+3)\hbar\omega$ space for the negative-parity states. In both sets of calculations all shells from the $0s$ to the $(0f1p)$ are used, with all particles active. In these cases the spectra were found again using the OXBASH program but with the WBP interaction of Warburton and Brown [49]. The resultant shell-model spectrum, together with the known spectra for ^{17}O and ^{17}F [29], is shown in Fig. 10. It is clear that the spectrum obtained from the shell model compares reasonably well with both spectra. Discrepancies between the model and the known spectra may be due to limitations in the model space and/or the underlying limitation on the ground state of ^{16}O. Nevertheless, this result serves to illustrate that the extreme single-particle picture of the mass-17 system is too simplistic. It points to the need for a coupled-channel description of the nuclei, with a possibly extended set of (^{16}O) target states to be included in the coupling scheme.

Figure 10 compares the low-energy shell-model spectrum of ^{17}F with that of MCAS, using parameters as per Table I, except with $V_0^- = -47.89$ MeV and $V_0^+ = -50.062$ MeV. This small change is made to account for the slight overbinding observed upon use of mirror symmetry.

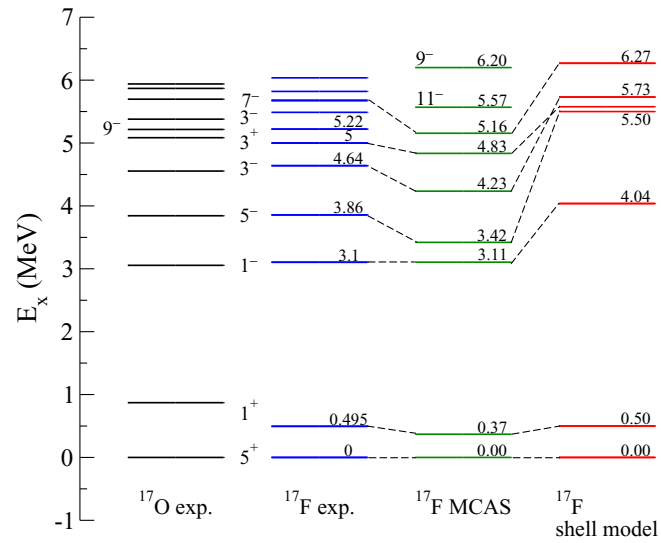

FIG. 10. Spectra for ^{17}O and ^{17}F [29], with zero energy corresponding to the ground states of each. The state labels denote $2J^\pi$.

APPENDIX B: THE VIBRATION MODEL FOR COUPLED-CHANNEL POTENTIALS

The surface of a liquid drop of incompressible fluid that can be slightly deformed is represented as

$$R(\theta\phi) = R_0\left[1 + \sum_{\lambda>1,\mu} \alpha^\star_{\lambda\mu} Y_{\lambda\mu}(\theta\phi)\right] = R_0[1+\varepsilon]. \quad \text{(B1)}$$

With this specification of the nuclear surface, expansion to second order in the coupling of a function gives

$$f(r) = f_0(r) + \varepsilon\left(\frac{\partial f(r)}{\partial\varepsilon}\right)_0 + \frac{1}{2}\varepsilon^2\left(\frac{\partial^2 f(r)}{\partial\varepsilon^2}\right)_0. \quad \text{(B2)}$$

Then, with ε as identified by Eq. (B1), and treating $R(\theta,\phi)$ as the variable in $f(r) = f(r - R(\theta,\phi))$,

$$\begin{aligned} f(r) = f_0(r) &- R_0 \sum_{\lambda\mu} \alpha^\star_{\lambda\mu} Y_{\lambda\mu}(\theta,\phi)\left(\frac{\partial f(r)}{\partial r}\right)_0 \\ &+ \frac{1}{2}R_0^2 \sum_{l_1 m_1 l_2 m_2} \alpha^\star_{l_1 m_1}\alpha^\star_{l_2 m_2} Y_{l_1 m_1}(\theta,\phi) \\ &\times Y_{l_2 m_2}(\theta,\phi)\left(\frac{\partial^2 f(r)}{\partial r^2}\right)_0. \end{aligned} \quad \text{(B3)}$$

Similar forms exist for $g(r) = \frac{1}{r}\frac{\partial f(r)}{\partial r}$, which is the usual function taken for spin-orbit terms. Therein, and in all that follows, it is presumed that summation of the expansion labels of the generalized coordinates, and subsequently of the angular-momentum quantum numbers of the phonon creation and annihilation operators derived from them, exclude dipole forms to ensure that there is no spurious center-of-mass motion associated with a scalar interaction.

The product of two generalized coordinates that satisfy the spherical harmonic condition can then be written as

$$\begin{aligned} \alpha^\star_{l_1 m_1}\alpha^\star_{l_2 m_2} &= \sum_{\nu_1\nu_2} \delta_{m_1\nu_1}\delta_{m_2\nu_2}\alpha^\star_{l_1\nu_1}\alpha^\star_{l_2\nu_2} \\ &= \sum_{\lambda\mu} \langle l_1 l_2 m_1 m_2|\lambda\mu\rangle\left[\alpha^\star_{l_1}\otimes\alpha^\star_{l_2}\right]_{\lambda\mu}, \\ \left[\alpha^\star_{l_1}\otimes\alpha^\star_{l_2}\right]_{\lambda\mu} &= \sum_{\nu_1\nu_2} \langle l_1 l_2 \nu_1\nu_2|\lambda\mu\rangle\alpha^\star_{l_1\nu_1}\alpha^\star_{l_2\nu_2}. \end{aligned} \quad \text{(B4)}$$

This form is convenient since $[\alpha^\star_{l_1}\otimes\alpha^\star_{l_2}]_{\lambda\mu}$ is a component of an irreducible tensor. Then, by using

$$\begin{aligned} &\sum_{m_1 m_2} \langle l_1 l_2 m_1 m_2|\lambda\mu\rangle Y_{l_1 m_1}(\theta,\phi)Y_{l_2 m_2}(\theta,\phi) \\ &\quad = \sqrt{\frac{(2l_1+1)(2l_2+1)}{4\pi(2\lambda+1)}}\langle l_1 l_2 00|\lambda 0\rangle Y_{\lambda\mu}(\theta,\phi), \end{aligned} \quad \text{(B5)}$$

the second-order term in Eq. (B3) can be written as

$$\begin{aligned} T_2 = \frac{1}{2}R_0^2\frac{\partial^2 f_0(r)}{\partial r^2} &\sum_{l_1 m_1 l_2 m_2 \lambda\mu K} \langle l_1 l_2 m_1 m_2|\lambda\mu\rangle\left[\alpha^\star_{l_1}\otimes\alpha^\star_{l_2}\right]_{\lambda\mu} \\ &\times\sqrt{\frac{(2l_1+1)(2l_2+1)}{4\pi(2K+1)}}\langle l_1 l_2 00|K0\rangle\langle l_1 l_2 m_1 m_2|K M_K\rangle \\ &\times Y_{K M_K}(\theta,\phi). \end{aligned} \quad \text{(B6)}$$

The orthogonality of Clebsch–Gordan coefficients reduces this to

$$\begin{aligned} T_2 = \frac{1}{2}R_0^2\frac{\partial^2 f_0(r)}{\partial r^2}&\sum_\lambda \sqrt{\frac{(2l_1+1)(2l_2+1)}{4\pi(2\lambda+1)}}\langle l_1 l_2 00|\lambda 0\rangle \\ &\times\left[\alpha^\star_{l_1}\otimes\alpha^\star_{l_2}\right]_\lambda\cdot\mathbf{Y}_\lambda(\theta,\phi), \end{aligned} \quad \text{(B7)}$$

since the generalized coefficients must satisfy the spherical harmonic condition.

Then the function form can be recast as

$$\begin{aligned} f(r) = f_0(r) &- R_0\left(\frac{\partial f(r)}{\partial r}\right)_0 \sum_\lambda \mathcal{Q}^{(1)}_\lambda\cdot Y_\lambda(\theta,\phi) \\ &+ \frac{1}{2}R_0^2\left(\frac{\partial^2 f(r)}{\partial r^2}\right)_0 \sum_\lambda\left[\sum_{l_1 l_2}\mathcal{Q}^{(2)}_\lambda(l_1 l_2)\right]\cdot Y_\lambda(\theta,\phi), \end{aligned} \quad \text{(B8)}$$

where $\mathcal{Q}^{(i)}_\lambda$ are the first- and (partial) second-order Tamura operators [50],

$$\begin{aligned} \mathcal{Q}^{(1)}_{\lambda\mu} &= \alpha^\star_{\lambda\mu}, \\ \mathcal{Q}^{(2)}_{\lambda\mu}(l_1 l_2) &= \sqrt{\frac{(2l_1+1)(2l_2+1)}{4\pi(2\lambda+1)}}\langle l_1 l_2 00|\lambda 0\rangle\left[\alpha^\star_{l_1}\otimes\alpha^\star_{l_2}\right]_{\lambda\mu}. \end{aligned} \quad \text{(B9)}$$

1. The nucleus as a quantized liquid drop

With the surface of a liquid drop of incompressible fluid that can be slightly deformed represented as in Eq. (B1), and with $\lambda \geqslant 2$, quantization proceeds by mapping the generalized coordinates ($\alpha_{\lambda\mu}$) and their canonical generalized momenta by using boson creation and annihilation operators $b^\dagger_{\lambda\mu}$ and $b_{\lambda\mu}$ by

$$\alpha_{\lambda\mu} \Rightarrow \sqrt{\frac{\hbar}{2B_\lambda\omega_\lambda}}[b_{\lambda\mu} + (-)^\mu b^\dagger_{\lambda-\mu}]. \quad \text{(B10)}$$

With a similar form for the generalized momentum, the Hamiltonian for a vibrating liquid (quantal) drop is

$$H = \sum_{\lambda\mu}\left[b^\dagger_{\lambda\mu}b_{\lambda\mu} + \frac{1}{2}\right]\hbar\omega_\lambda, \quad \text{where } [b_{\lambda\mu}, b^\dagger_{\lambda'\mu'}] = \delta_{\lambda\lambda'}\delta_{\mu\mu'}. \quad \text{(B11)}$$

Then, normalized one- and two-phonon states are defined by

$$\begin{aligned} |1;\lambda\mu\rangle &= b^\dagger_{\lambda\mu}|0\rangle, \\ |2;(\lambda_1\lambda_2)JM\rangle &= \frac{1}{\sqrt{1+\delta_{\lambda_1\lambda_2}}}\left[b^\dagger_{\lambda_1}\otimes b^\dagger_{\lambda_2}\right]_{JM}|0\rangle, \end{aligned} \quad \text{(B12)}$$

where

$$\left[b^\dagger_{\lambda_1}\otimes b^\dagger_{\lambda_2}\right]_{JM} = \sum_{m_1 m_2}\langle\lambda_1\lambda_2\mu_1\mu_2|JM\rangle b^\dagger_{\lambda_1\mu_1}b^\dagger_{\lambda_2\mu_2}. \quad \text{(B13)}$$

This model involves generalized mass and restoring force parameters (B_λ, C_λ) with which the frequencies of the phonons

and the coupling parameters are

$$\omega_\lambda = \sqrt{\frac{C_\lambda}{B_\lambda}}, \quad \beta_\lambda = \sqrt{(2\lambda+1)}(a_\lambda)_0 = |\langle 1\|\alpha_\lambda\|0\rangle| = \sqrt{(2\lambda+1)}\sqrt{\frac{\hbar}{2B_\lambda\omega_\lambda}}. \tag{B14}$$

Here $(a_\lambda)_0$ is the zero-point amplitude of vibration [6,51].

2. The vibration model for coupled-channel interactions

With channels $c = \{lj; I; JM\}$ as used in the MCAS theory of a nucleon interacting with a nucleus [7], matrix elements of the type

$$\begin{aligned}[f(r)]_{cc'} = [f_0(r)]_{cc'} &- R_0\left[\frac{\partial f(r)}{\partial r}\sum_\lambda\left[\alpha^\star_\lambda\cdot Y_\lambda(\theta\phi)\right]\right]_{cc'} \\ &+ \frac{1}{2}R_0^2\left[\left(\frac{\partial^2 f(r)}{\partial r^2}\right)_0\sum_\lambda\sum_{l_1l_2}\sqrt{\frac{(2l_1+1)(2l_2+1)}{4\pi(2\lambda+1)}}\langle l_1l_200|\lambda0\rangle\left[\alpha^\star_{l_1}\otimes\alpha^\star_{l_2}\right]_\lambda\cdot Y_\lambda(\theta\phi)\right]_{cc'}\end{aligned} \tag{B15}$$

are required. We choose to use as the basic interaction potential form

$$f_0(r) = [V_0 + V_{ll}\{\mathbf{l}\cdot l\} + V_{ss}\{\mathbf{I}\cdot s\}]w(r) + 2\lambda_\pi^2 V_{ls}\frac{1}{r}\frac{\partial w(r)}{\partial r}\{\mathbf{l}\cdot s\}. \tag{B16}$$

A Woods–Saxon form, $w(r) = [1+\exp(\frac{r-R_0}{a})]^{-1}$ is used.

Each operator character of the interaction has zero-, first-, and second-order elements due to the expansion in deformation. Thus for each term in the interaction, form factors in whatever channel coupling can be specified as

$$V_{cc'}(r) = \{V^{(0)}(r)\}_{cc'} + \left\{V^{(1)}(r)\sum_\lambda\mathcal{Q}^{(1)}_\lambda\cdot Y_\lambda(\theta\phi)\right\}_{cc'} + \left\{V^{(2)}(r)\sum_\lambda\left[\sum_{l_1l_2}\mathcal{Q}^{(2)}_\lambda(l_1,l_2)\right]\cdot Y_\lambda(\theta\phi)\right\}_{cc'}. \tag{B17}$$

With $W_{ls} = 2\lambda_\pi^2 V_{ls}$, the zero-order term in Eq. (B17) is

$$\{V^{(0)}(r)\}_{cc'} = \left\{\left[V_0^{(c)} + V_{ll}^{(c)}l(l+1)\right]w(r) + W_{ls}^{(c)}\frac{1}{r}\frac{\partial w(r)}{\partial r}\{\mathbf{l}\cdot\mathbf{s}\}\right\}\delta_{cc'} + \frac{1}{2}\left[V_{ss}^{(c)} + V_{ss}^{(c')}\right]w(r)\{\mathbf{I}\cdot\mathbf{s}\}_{\mathbf{cc'}}, \tag{B18}$$

and the superscripts on the potential strengths indicate that the values for the appropriate parities of the channel c are to be taken. Also, a symmetrized form is used for terms that allow coupling between different channels. Such is the case with the other two components and

$$\begin{aligned}\{V^{(1)}(r)\}_{cc'} = &\left\{-R_0\frac{\partial w(r)}{\partial r}\frac{1}{2}\left[V_0^{(c)} + V_0^{(c')} + V_{ll}^{(c)}\{\mathbf{l}\cdot\mathbf{l}\}_{cc} + V_{ll}^{(c')}\{\mathbf{l}\cdot\mathbf{l}\}_{c'c'}\right]\right. \\ &\left. - \frac{1}{2}R_0^2\frac{1}{r}\frac{\partial^2 w(r)}{\partial r^2}\left(W_{ls}^{(c)}\{\mathbf{l}\cdot\mathbf{s}\}_{cc} + W_{ls}^{(c')}\{\mathbf{l}\cdot\mathbf{s}\}_{c'c'}\right)\right\}\sum_L\left[\mathcal{Q}^{(1)}_L\cdot Y_L\right]_{cc'} \\ &- \frac{1}{2}R_0\frac{\partial w(r)}{\partial r}\sum_L\sum_{c''}\left\{V_{ss}^{(c')}\left[\mathcal{Q}^{(1)}_L\cdot Y_L\right]_{cc''}[\mathbf{I}\cdot\mathbf{s}]_{c''c'} + V_{ss}^{(c)}[\mathbf{I}\cdot\mathbf{s}]_{cc''}\left[\mathcal{Q}^{(1)}_L\cdot Y_L\right]_{c''c'}\right\}.\end{aligned} \tag{B19}$$

The second-order terms are

$$\begin{aligned}\{V^{(2)}(r)\}_{cc'} = &\left\{\frac{1}{4}R_0^2\frac{\partial^2 w(r)}{\partial r^2}\left[V_0^{(c)} + V_0^{(c')} + V_{ll}^{(c)}\{\mathbf{l}\cdot\mathbf{l}\}_{cc} + V_{ll}^{(c')}\{\mathbf{l}\cdot\mathbf{l}\}_{c'c'}\right]\right. \\ &\left. + \frac{1}{4}R_0^3\frac{1}{r}\frac{\partial^3 w(r)}{\partial r^3}\left(W_{ls}^{(c)}\{\mathbf{l}\cdot\mathbf{s}\}_{cc} + W_{ls}^{(c')}\{\mathbf{l}\cdot\mathbf{s}\}_{c'c'}\right)\right\}\sum_\lambda\left[\left\{\sum_{l_1l_2}\mathcal{Q}^{(2)}_\lambda(l_1,l_2)\right\}\cdot Y_\lambda\right]_{cc'} \\ &+ \frac{1}{4}R_0^2\frac{\partial^2 w(r)}{\partial r^2}\sum_\lambda\sum_{c''}\left[V_{ss}^{(c)}\{\mathbf{I}\cdot\mathbf{s}\}_{cc''}\left[\left\{\sum_{l_1l_2}\mathcal{Q}^{(2)}_\lambda(l_1,l_2)\right\}\cdot Y_\lambda\right]_{c''c'}\right. \\ &\left. + V_{ss}^{(c')}\left[\left\{\sum_{l_1l_2}\mathcal{Q}^{(2)}_\lambda(l_1,l_2)\right\}\cdot Y_\lambda\right]_{cc''}\{\mathbf{I}\cdot\mathbf{s}\}_{c''c'}\right].\end{aligned} \tag{B20}$$

The matrix elements of the operators $\{\mathbf{l}\cdot\mathbf{l}\}$, $\{\mathbf{I}\cdot\mathbf{s}\}$, and $\{\mathbf{l}\cdot\mathbf{s}\}$ have been defined previously [7]. And, as the first- and second-order terms require development as matrix elements of nuclear operators, we use the Edmond's form of the Wigner–Eckart theorem, i.e.,

$$\langle J_f M_f|T_{LM}|J_i M_i\rangle = \frac{1}{\sqrt{(2J_f+1)}}\langle J_i L M_i M|J_f M_f\rangle\langle J_f||T_L||J_i\rangle. \tag{B21}$$

For the case of scalar operators to be used herein (so conserving total angular momentum $J = J'$), specifically with the Tamura operators cast temporarily as a general operator $\mathcal{Q}$, we use $T_{0,0} = [\mathcal{Q}_L\cdot Y_L]_{0,0}$, so that

$$\langle c|[\mathcal{Q}_L\cdot Y_L]_{0,0}|c'\rangle = \frac{1}{\sqrt{(2J+1)}}\,\langle c||[\mathcal{Q}_L\cdot Y_L]_0||c'\rangle, \tag{B22}$$

for all M as the Clebsch–Gordan coefficient is a δ function. Then using a Brink and Satchler identity [Eq. (5.13) in Ref. [52]], suitably adjusted to Edmond's form for the Wigner–Eckart theorem, i.e.,

$$\langle c||[\mathcal{Q}_L\cdot Y_L]||c'\rangle = \langle (jI)J||[\mathcal{Q}_L\cdot Y_L]||(j'I')J\rangle = (-)^{j'+I+J}\begin{Bmatrix} j & j' & L\\ I' & I & J\end{Bmatrix}\frac{1}{\sqrt{(2J+1)}}\langle j||Y_L||j'\rangle\langle I||\mathcal{Q}_L||I'\rangle, \tag{B23}$$

and as

$$\langle j||Y_L||j'\rangle = (-)^{j+L-j'}\sqrt{\frac{(2L+1)(2j'+1)}{4\pi}}\langle j' L\tfrac{1}{2}0|j\tfrac{1}{2}\rangle, \tag{B24}$$

$$\langle c||[\mathcal{Q}_L\cdot Y_L(\Omega)]||c'\rangle = (-)^{j+L+I+J}\begin{Bmatrix} j & j' & L\\ I' & I & J\end{Bmatrix}\sqrt{\frac{(2j'+1)(2L+1)}{4\pi(2J+1)}}\langle j' L\tfrac{1}{2}0|j\tfrac{1}{2}\rangle\langle I||\mathcal{Q}_L||I'\rangle. \tag{B25}$$

Thus to specify all terms in the form for the interaction matrix of potentials, Eq. (B20), the reduced matrix elements of the various Tamura operators [50] are required.

[1] K. Mizuyama and K. Ogata, Phys. Rev. A **86**, 041603(R) (2012).
[2] G. Blanchon, M. Dupuis, H. F. Arellano, and N. Vinh Mau, Phys. Rev. C **91**, 014612 (2015).
[3] T. V. Nhan Hao, Bai Minh Loc, and Nguyen Hoang Phuc, Phys. Rev. C **92**, 014605 (2015).
[4] K. Mizuyama, G. Colò, and E. Vigezzi, Phys. Rev. C **86**, 034318 (2012).
[5] G. P. A. Nobre, F. S. Dietrich, J. E. Escher, I. J. Thompson, M. Dupuis, J. Terasaki, and J. Engel, Phys. Rev. Lett. **105**, 202502 (2010).
[6] A. Bohr and B. R. Mottelson, *Nuclear Structure: Vol II* (W. A. Benjamin, Massachusetts, 1975).
[7] K. Amos, L. Canton, G. Pisent, J. P. Svenne, and D. van der Knijff, Nucl. Phys. A **728**, 65 (2003).
[8] L. Canton, G. Pisent, J. P. Svenne, D. van der Knijff, K. Amos, and S. Karataglidis, Phys. Rev. Lett. **94**, 122503 (2005).
[9] L. Canton, G. Pisent, K. Amos, S. Karataglidis, J. P. Svenne, and D. van der Knijff, Phys. Rev. C **74**, 064605 (2006).
[10] L. Canton, G. Pisent, J. P. Svenne, K. Amos, and S. Karataglidis, Phys. Rev. Lett. **96**, 072502 (2006).
[11] K. Amos, L. Canton, P. R. Fraser, S. Karataglidis, J. P. Svenne, and D. van der Knijff, Nucl. Phys. A **879**, 132 (2012).
[12] G. E. Brown and A. M. Green, Nucl. Phys. **75**, 401 (1966).
[13] W. C. Haxton and C. Johnson, Phys. Rev. Lett. **65**, 1325 (1990).
[14] S. Karataglidis, P. J. Dortmans, K. Amos, and R. de Swiniarski, Phys. Rev. C **53**, 838 (1996).
[15] K. Amos, L. Canton, P. R. Fraser, S. Karataglidis, J. P. Svenne, and D. van der Knijff, Nucl. Phys. A **912**, 7 (2013).
[16] K. Amos, S. Karataglidis, D. van der Knijff, L. Canton, G. Pisent, and J. P. Svenne, Phys. Rev. C **72**, 064604 (2005).
[17] H. de Vries, C. W. de Jager, and C. de Vries, At. Data Nucl. Data Tables **36**, 495 (1987).
[18] J. Mitroy and G. Ryzhikh, Comput. Phys. Commun. **123**, 103 (1999).
[19] I. Ivanov, M. Bromley, and J. Mitroy, Comput. Phys. Commun. **152**, 9 (2003).
[20] D. C. Cuong, D. T. Khoa, and G. Colò, Nucl. Phys. A **836**, 11 (2010).
[21] S. Raman, C. W. Nestor Jr, and P. Tikkanen, At. Data Nucl. Data Tables **78**, 1 (2001).
[22] Y. Wu, S. Ishikawa, and T. Sasakawa, Phys. Rev. Lett. **64**, 1875 (1990).
[23] B. A. Brown, W. A. Richter, and R. Lindsay, Phys. Lett. B **483**, 49 (2000).
[24] M. Ohkubo, JAERI-M Reports **86**, 193 (1987); the paper is available at http://www.iaea.org and the data at http://www.nndc.bnl.gov.
[25] S. Cierjacks, F. Hinterberger, G. Schmalz, D. Erbe, P. V. Rossen, and B. Leugers, Nucl. Instrum. Methods **169**, 185 (1980).
[26] F. L. Fowler, C. H. Johnson, and R. M. Feezel, Phys. Rev. C **8**, 545 (1973).
[27] D. C. Larson, J. A. Harvey, and N. W. Hill, in *Symposium on Neutron Cross Sections 10–50 MeV* (Brookhaven, 1980), p. 277.
[28] M. Igashira, H. Kitazawa, and K. Takaura, Nucl. Phys. A **536**, 285 (1992).
[29] D. R. Tilley, H. R. Weller, and C. M. Cheves, Nucl. Phys. A **A564**, 1 (1993).
[30] M. Braun and T. Fried, Z. Phys. A: At. Nucl. (1975) **311**, 173 (1983).

[31] A. R. Ramos, A. Paúl, L. Rijniers, M. F. da Silva, and J. C. Soares, Nucl. Instrum. Methods Phys. Res., Sect. B **190**, 95 (2002).
[32] P. Fraser, K. Amos, L. Canton, D. van der Knijff, S. Karataglidis, and J. P. Svenne, Eur. Phys. J. A **51**, 110 (2015).
[33] N. Stone, At. Data Nucl. Data Tables **90**, 75 (2005).
[34] B. S. Ishkhanov and V. N. Orlin, Phys. Atom. Nuclei **68**, 1352 (2005).
[35] R. Spear, At. Data Nucl. Data Tables **42**, 55 (1989).
[36] T. Kibedi and R. Spear, At. Data Nucl. Data Tables **89**, 77 (2005).
[37] J. P. Davidson, *Collective Models of the Nucleus* (Academic Press, New York, 1968).
[38] C. P. Swann, Nucl. Phys. A **150**, 300 (1970).
[39] H. Miska *et al.*, Phys. Lett. B **59**, 441 (1975).
[40] K. Amos, R. de Swiniarski, and L. Berge, Nucl. Phys. A **485**, 653 (1988).
[41] A. Arima, P. Manakos, and D. Strottman, Phys. Lett. B **60**, 1 (1975).
[42] C. E. Rolfs, *Cauldrons in the Cosmos* (The University of Chicago Press, New Jersey, 1996).
[43] D. Roubtsov, K. Kozier, J. Chow, A. Plompen, S. Kopecki, J. P. Svenne, and L. Canton, Nucl. Data Sheets **118**, 414 (2014).
[44] S. Cohen and D. Kurath, Nucl. Phys. **73**, 1 (1965).
[45] B. A. Brown and D. H. Wildenthal, Annu. Rev. Nucl. Part. Sci. **38**, 29 (1988).
[46] D. J. Millener and D. Kurath, Nucl. Phys. A **255**, 315 (1975).
[47] T. Kuo and G. Brown, Nucl. Phys. **85**, 40 (1966).
[48] T. Kuo and G. Brown, Nucl. Phys. A **114**, 241 (1968).
[49] E. K. Warburton and B. A. Brown, Phys. Rev. C **46**, 923 (1992).
[50] T. Tamura, Rev. Mod. Phys. **37**, 679 (1965).
[51] W. Greiner and J. A. Maruhn, *Nuclear Models* (Springer-Verlag, Berlin, 1996).
[52] D. M. Brink and G. R. Satchler, *Angular Momentum* (Clarendon Press, Oxford, 1968).